

RSC Advances



This is an *Accepted Manuscript*, which has been through the Royal Society of Chemistry peer review process and has been accepted for publication.

Accepted Manuscripts are published online shortly after acceptance, before technical editing, formatting and proof reading. Using this free service, authors can make their results available to the community, in citable form, before we publish the edited article. This *Accepted Manuscript* will be replaced by the edited, formatted and paginated article as soon as this is available.

You can find more information about *Accepted Manuscripts* in the [Information for Authors](#).

Please note that technical editing may introduce minor changes to the text and/or graphics, which may alter content. The journal's standard [Terms & Conditions](#) and the [Ethical guidelines](#) still apply. In no event shall the Royal Society of Chemistry be held responsible for any errors or omissions in this *Accepted Manuscript* or any consequences arising from the use of any information it contains.

Energy and dose dependence of proton-irradiation damage in graphene

Gwangseok Yang¹, Byung-Jae Kim¹, Kyeounghak Kim², Jeong Woo Han^{2,*}, and Jihyun Kim^{1,*}

¹Department of Chemical and Biological Engineering, Korea University, Seoul 136-713
Korea

²Department of Chemical Engineering, University of Seoul, Seoul 130-743 Korea

Abstract

Monolayer graphenes were irradiated with 5–15 MeV high-energy protons at various doses from 1×10^{16} to 3×10^{16} cm⁻², and their characteristics were systematically investigated using micro-Raman spectroscopy and X-ray photoelectron spectroscopy (XPS). As the energy and dose of the proton irradiation increased, the defects induced in the graphene layers also increased gradually. The average defect distances of 10 MeV proton-irradiated graphene decreased to 29 ± 5 nm at a dose of 3×10^{16} cm⁻². The defect formation energies for various types of defects were compared by using density functional theory calculation. After proton irradiation, the results of micro-Raman scattering and XPS indicated p-doping effects due to adsorption of environmental molecules on the damaged graphene. Our results show a direct relationship between the defect formation of the graphene layers and the energy/dose of the proton irradiation.

Keywords: graphene; proton irradiation; defects

Corresponding authors: Tel: +82-2-3290-3291, E-mail: hyunhyun7@korea.ac.kr (Jihyun Kim) and Tel: +82-2-6490-2373, E-mail: jwhan@uos.ac.kr (Jeong Woo Han)

1. Introduction

Protons with energies up to hundreds of MeV found in the earth's magnetic field can cause malfunctioning and deterioration of electronic devices used in space.¹⁻³ The interactions between high-energy particles and semiconductor thin films mainly include ionization and displacement damage. When highly energetic particles collide with crystalline thin films, they generally create vacancy–interstitial pairs, which are considered to be point defects. Because they are mobile even at room temperature, the radiation-induced defects can be annihilated by recombination or form defect complexes or secondary defects.¹ When exposed to high-energy bombardment for an extended period, the crystalline structures eventually turn into amorphous materials, which are not desirable in terms of device performance and reliability. Because radiation-induced degradation threatens the lifetime of electronic components used in space applications, knowledge of the degradation mechanism of electronic devices under proton irradiation is essential to improve their long-term reliability. To gain such knowledge, graphene is an ideal material because it is a densely packed planar monolayer with sp^2 -bonded carbon atoms. Two-dimensional structure of graphene allows the fundamental studies of radiation-induced damage and degradation mechanism in ultra-thin films, which are the building blocks of next-generation electronic devices.

Graphene has become an attractive material for uses in nanoelectronics, energy materials, nanosensors, and optoelectronics because of its fascinating properties, such as ultrahigh carrier mobility, superior thermal/electrical conductivity, exceptional optical transparency, and high mechanical strength.⁴⁻¹⁰ Defects in graphene layers significantly change its structural, electronic, and magnetic properties, especially in monolayer graphene, where all the atoms are surface atoms.¹¹⁻¹⁴ The controlled introduction of defects into

graphene can create a bandgap, which is absent in pristine graphene.¹² The optical and morphological properties of carbon nanotubes (CNTs) after proton irradiation have been investigated.^{15, 16} CNT-based field-effect transistors were very tolerant of proton irradiation at energies of 10–35 MeV up to doses of $4 \times 10^{12} \text{ cm}^{-2}$.¹⁷ However, proton-irradiated graphene has rarely been investigated. Mathew et al. investigated the effects of 2 MeV proton irradiation on mono- and few-layer graphene, where the threshold proton dose in monolayer graphene was approximately $1 \times 10^{16} \text{ cm}^{-2}$.¹⁸ They also reported that the damage induced by proton irradiation depends on both the number of graphene layers and the underlying substrate.¹⁹ Ko et al. reported a decrease in the hole mobility of few-layer graphene after proton irradiation at an energy of 5 MeV and doses up to $2 \times 10^{15} \text{ cm}^{-2}$, where the graphene was obtained by mechanical cleavage of highly oriented pyrolytic graphite.²⁰ In this letter, we investigated the effects of high-energy (5–15 MeV) proton irradiation on monolayer graphene grown by chemical vapor deposition technique. In addition, the effects of various doses (1×10^{16} – $3 \times 10^{16} \text{ cm}^{-2}$) at an energy of 10 MeV were systematically studied using micro-Raman scattering and X-ray photoelectron spectroscopy (XPS).

2. Experimental details

Monolayer graphene deposited on Cu foil by chemical vapor deposition technique was used in our experiment. Our wet-transfer method is as follows: Poly(methyl methacrylate) (PMMA), which was dissolved in chlorobenzene (46 mg/ml, Sigma-Aldrich), was spin-coated on a graphene layer on the front side of the Cu foil and heated at 180 °C for 5 min to cure the PMMA layer. Subsequently, graphene that was grown on the back side of the Cu foil was removed by reactive-ion etching using O₂ plasma for 5 s. The PMMA/graphene/Cu foil

structure was floated on a Cu etchant (1 wt.% of ammonium persulfate dissolved in deionized water) for 8 h. After the PMMA-coated graphene was transferred onto a SiO₂/Si substrate, the PMMA layer was removed in acetone, yielding the structure of monolayer graphene/SiO₂/Si substrate.

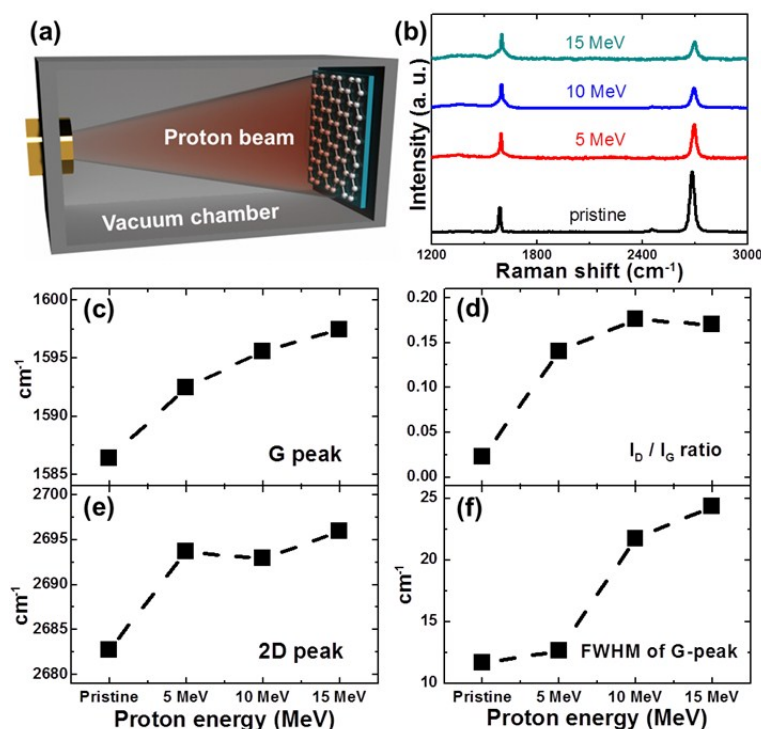


Figure 1. (a) Schematic diagram of proton irradiation of monolayer graphene/SiO₂/Si substrate inside the vacuum chamber, (b) Raman spectra of graphene before and after 5–15 MeV proton irradiation with a dose of $1 \times 10^{16} \text{ cm}^{-2}$, (c) position of G peak, (d) intensity ratio of D to G peak (I_D/I_G), (e) position of 2D peak, and (f) FWHM of G peak plotted for pristine and proton-irradiated graphene at different proton irradiation energies.

Proton irradiation was performed using the MC-50 cyclotron at the Korea Institute of Radiological and Medical Sciences. Figure 1 (a) is a schematic diagram of proton irradiation of monolayer graphene. The energy of the proton beam from the MC-50 cyclotron was

initially 20 MeV and was adjusted by an aluminum degrader to range from 5 to 15 MeV inside a low-vacuum chamber where the pressure was maintained at 2.5×10^{-2} Torr. The beam current (200 nA) was measured using a Faraday cup, and the irradiation time (5089 s) was used to calculate the fluence. The dose was fixed at 1×10^{16} cm⁻² at each irradiation step for various proton energies (5–15 MeV). Proton irradiation with a fixed proton energy of 10 MeV and proton dose of 1×10^{16} cm⁻² was repeated to achieve a fluence of 3×10^{16} cm⁻², which allows us to study the effects of the proton dose on the degradation of the graphene layer. Micro-Raman spectroscopy (Horiba Jobin Yvon, LabRam Aramis) in a back-scattering geometry using a 514.5 nm line of an Ar-ion laser at room temperature was used to investigate the disorder in the graphene. XPS (Thermo, K-alpha) using the monochromated Al K α line as the X-ray source was employed to study the changes in the bonding structure of the graphene layer after proton bombardment. The binding energy information was collected in a circular area (400 μ m in diameter).

We performed plane-wave density functional theory (DFT) calculations using the Vienna ab initio Simulation Package (VASP).^{21,22} Exchange-correlation energies were treated by Perdew-Burke-Ernzerhof (PBE) function based on generalized gradient approximation (GGA).²³ A plane wave expansion with a cutoff of 400 eV was used with a $2 \times 2 \times 1$ Monkhorst-Pack²⁴ k-point sampling of the Brillouin zone, which was sufficient to give well converged results. Total energy calculations used the residual minimization method for electronic relaxation and geometries were relaxed using a conjugate gradient algorithm until the forces on all unconstrained atoms were less than 0.03 eV/Å. In order to take into account for dispersion force, we used semi-empirical DFT-D2 method proposed by Grimme.²⁵ We used a graphene unit cell of 72 carbon atoms. The x - y size of the supercell was $14.80 \text{ \AA} \times 12.82 \text{ \AA}$. The vacuum thickness of 17 Å was used to decouple the periodic images of the slab

surfaces. The defect formation energy of graphene (E_f) was calculated from the total energies of the supercells with a defect,²⁶

$$E_f = E_d - E_p - n\mu \quad (1)$$

where E_d is the total energy of the system containing the defects, E_p is the total energy for the optimized pristine graphene, μ is the chemical potential of carbon atom, and n is the number of carbon atoms that were added or removed from the pristine graphene.

3. Results and discussion

Figure 1 (b) shows the evolution of Raman spectra of the graphene before and after proton irradiation with energies of 5, 10, and 15 MeV at a fixed dose of $1 \times 10^{16} \text{ cm}^{-2}$. The Raman spectra of pristine graphene generally had two main peaks: the G peak ($\sim 1585 \text{ cm}^{-1}$) and the 2D peak ($\sim 2680 \text{ cm}^{-1}$). The thickness of the pristine graphene was estimated using the typical features of monolayer graphene: (i) a 2D-to-G-peak intensity ratio of ~ 2.3 and (ii) a symmetric 2D band centered at 2683 cm^{-1} with a full-width-at-half-maximum (FWHM) of $\sim 28 \text{ cm}^{-1}$.²⁷ In addition, the D peak at $\sim 1356 \text{ cm}^{-1}$, which reflects the existence of the Raman active defects, was ignorable in the case of pristine graphene, as shown in fig. 1 (b). In fig. 1 (d), the intensity ratio (I_D/I_G) of the D peak to the G peak, which serves as the conventional criterion for analyzing defects or disorder in graphene,^{11,28} increases from 0.02 to 0.17 with increasing proton energy. In addition, the changes in the FWHM of the G peak indicate structural disordering of the graphene with increasing proton energy,^{28, 29} although the FWHM of the G peak can vary with the doping of graphene.³⁰ As shown in fig. 1 (f), the FWHM of the G peak increased from 12 cm^{-1} to 24 cm^{-1} , which can be explained by the

increase in the defect density after 15 MeV proton irradiation. Therefore, the disorder in the graphene increased with increasing proton irradiation energy up to 15 MeV in our experiment. Figures 1(c) and 1(e) show that proton irradiation shifted the G and 2D peaks upward, which implies unintentional chemical doping of the graphene when the irradiated samples were stored in an air ambient. The doping polarity can be determined by correlating the peak positions of the G and 2D bands, where the upshifts of both the G and 2D peaks indicate p-doping by charge transfer between the adsorbed molecules and the graphene.^{31,32}

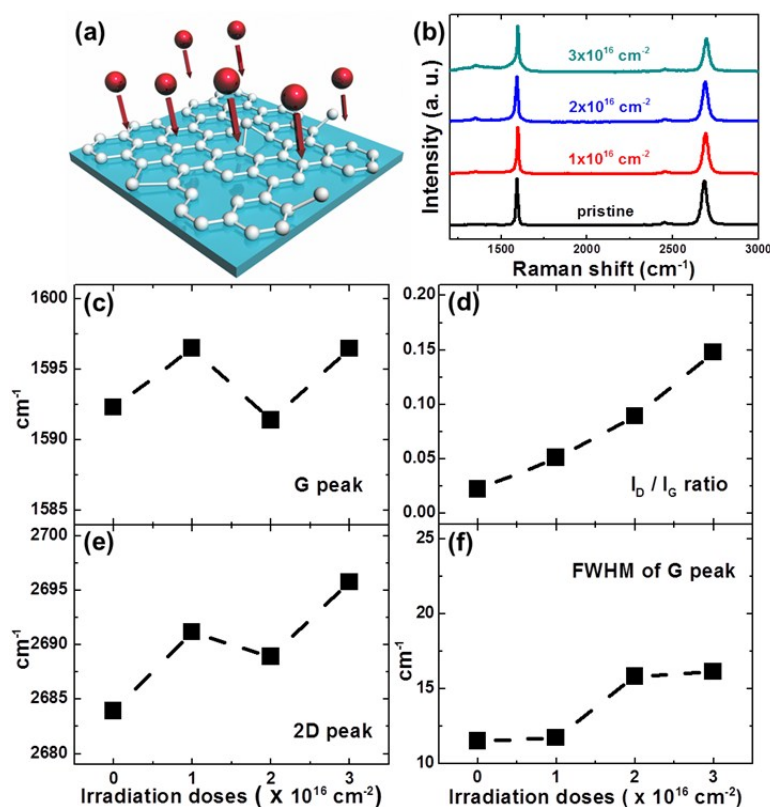


Figure 2. (a) Schematic diagram of defective graphene under proton irradiation, (b) Raman spectra of graphene before and after 10 MeV proton irradiation with doses of 1×10^{16} to $3 \times 10^{16} \text{ cm}^{-2}$, (c) position of G peak, (d) intensity ratio of D to G peak (I_D/I_G), (e) position of 2D peak, and (f) FWHM of G peak plotted for pristine and proton-irradiated graphene at varying

doses.

Disorder induced by proton irradiation is schematically illustrated in fig. 2 (a). The amorphization trajectory of carbon materials when defects were introduced was previously reported using Raman spectroscopy.^{28, 33, 34} Figure 2 (b) shows the evolution of Raman spectra of graphene before and after 10 MeV proton irradiation with various doses from 1×10^{16} to $3 \times 10^{16} \text{ cm}^{-2}$. The characteristics of high-quality monolayer graphene were confirmed by three features: (i) the 2D-to-G-peak intensity ratio is ~ 1 , (ii) the symmetric 2D band is centered at 2681 cm^{-1} with an FWHM of $\sim 35 \text{ cm}^{-1}$, and (iii) the D peak at 1350 cm^{-1} is ignorable. Figures 2(d) and 2(f) show that I_D/I_G is consistent with the FWHM of the G peak at increasing doses, indicating more damage at higher doses. In figs. 2(c) and 2(e), the positions of the G and 2D peaks imply p-doping of the irradiated graphene for the reasons mentioned above. Figure 2 (d) shows that I_D/I_G increases with increasing proton irradiation dose owing to the increase in the defect density. Under a low-defect-density regime [L_D (average defect distance) $\geq 10 \text{ nm}$], since the ratio of I_D/I_G is inversely proportional to L_D^2 , L_D can be estimated by using the equation,³⁴

$$L_D^2 (\text{nm}^2) = (1.8 \pm 0.5) \times 10^{-9} \times \lambda_L^4 \times \left(\frac{I_D}{I_G}\right)^{-1} \quad (2)$$

where λ_L is the excitation laser wavelength. The L_D values of our pristine graphene and 10 MeV proton-irradiated graphenes with doses of 1×10^{16} , 2×10^{16} , and $3 \times 10^{16} \text{ cm}^{-2}$ are 76 ± 11 , 50 ± 7 , 37 ± 5 , and $29 \pm 5 \text{ nm}$, respectively. Therefore, we could confirm that the defect density is proportional to the proton dose. The change in the FWHM of the G peak with increasing proton dose is shown in fig. 2 (f). Because the FWHM of the G peak increases

with increasing dose, the results from fig. 2 (d) are consistent with those from fig. 2 (f), indicating increased disorder at higher doses.

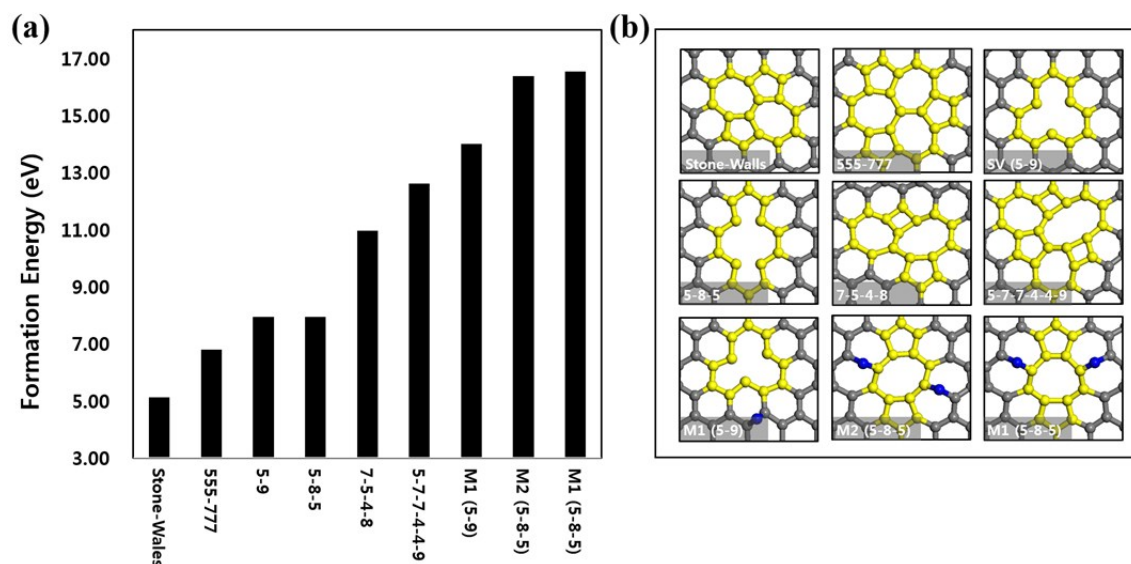


Figure 3. (a) Defect formation energies of various defect models. (b) The reconstructed models are Stone-wales, 7-5-4-8 and 5-7-7-4-4-9 (topological defects). The vacancy models are 5-9 (single vacancy), 5-8-5, and 555-777 (double vacancies). The adatom-vacancy pair models are M1 (SV or 5-9), M1 (5-8-5), and M2 (5-8-5). Normal C atoms are shown as gray spheres, defect region as yellow spheres, and adatoms as blue spheres, respectively.

In order to identify the type of defects induced by proton irradiation, we performed DFT calculations. The formation of various types of defects was compared by calculating the defect formation energies as described in Eq. (1). With this definition, lower defect formation energy implies easier formation of the defect. We considered three types of defect models as reported in previous literatures (fig. 3 (b)); reconstructed, vacancy, and adatom-vacancy pair models. The formation energy of each defect is summarized in fig. 3 (a). First, reconstructions are occurred by rotating or breaking and recombination of C-C bonds. The

possible models are stone-walls (SW) ($E_f = 5.11$ eV) and 7-5-4-8 ($E_f = 10.96$ eV) and 5-7-7-4-4-9 ($E_f = 12.61$ eV) models.^{12, 35-38} The 7-5-4-8 and 5-7-7-4-4-9 models contain two different shapes of rectangle and octagon, instead of normal hexagon. Meanwhile, the SW defect is formed by 90° rotation of only one C-C bond. This exhibits the smallest defect formation energy, implying the most probable defect to be formed among the various defects we examine. Second, vacancy models involve the formation of carbon vacancy. The single vacancy (SV or 5-9) misses one lattice carbon atom ($E_f = 7.94$ eV) while the double vacancy (5-8-5) loses the adjacent two lattice carbon atoms ($E_f = 7.94$ eV).^{12, 35, 39, 40} Both models break C-C bonds to form the dangling bonds involved in a void area. The 555-777 ($E_f = 6.80$ eV) is also related to the missing of two lattice carbon atoms, but followed by the formation of vacancies, the rearrangement of carbon atoms near the vacancies is additionally occurred without breaking the C-C bonds. Last, adatom-vacancy pair models include both vacancy and adatom (interstitial) atoms, which has been experimentally observed before.⁴¹ The M1 (SV or 5-9) model ($E_f = 13.99$ eV) has a pair form of one SV vacancy and one carbon adatom on the interstitial site while the M1 (5-8-5) ($E_f = 16.52$ eV) and M2 (5-8-5) ($E_f = 16.38$ eV) models are involved in two 5-8-5 vacancies and two adatoms on the adjacent interstitial sites. Since these models involve two processes of creating vacancies and then moving them to the nearby interstitial sites as adatoms, high defect formation energies (>13 eV) are required, compared to the other defect models. In the view of thermodynamics, the energy required to form one more carbon vacancy from SV to 5-8-5 in the vacancy models is almost zero. However, the adatom-vacancy pair model (M1 or M2) can be approximately considered as a transition states of the process, which is energetically higher than SV by ~ 8.5 eV. Thus, the process from SV to 5-8-5 is not a barrier-free process. Based on our DFT results, the defects formed by reconstructing the C-C bonds such as SW would occupy the large portion of

defects created on the monolayer graphene after proton irradiation. However, the types of the defects might have less dependence on E_f because the proton irradiation energy is much higher than E_f . Incident angle and irradiation energies also need to be considered.^{42, 43}

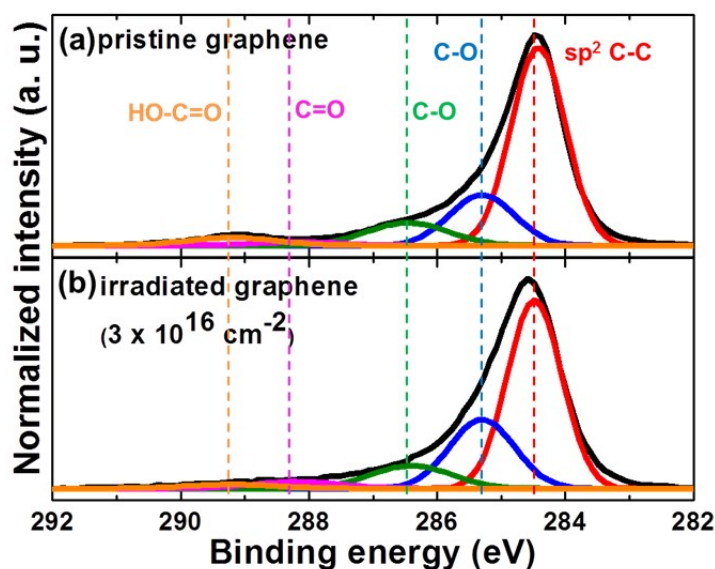


Figure 4. XPS data of C1s core level for (a) pristine and (b) 10 MeV proton-irradiated graphene at a dose of $3 \times 10^{16} \text{ cm}^{-2}$.

The changes in the chemical bonding states of the graphene by proton irradiation were analyzed by XPS. Figures 4(a) and 4(b) show the C1s core-level XPS spectra of the graphene layer before and after 10 MeV proton irradiation with a dose of $3 \times 10^{16} \text{ cm}^{-2}$, respectively. The C1s core peaks were divided into five symmetric Gaussian curves: a predominant sp² C–C (binding energy $E_B = 284.4 \text{ eV}$), C–O ($E_B = 285.3 \text{ eV}$), C–O ($E_B = 286.4 \text{ eV}$), C=O ($E_B = 288.2 \text{ eV}$), and HO–C=O ($E_B = 289.2 \text{ eV}$).^{44, 45} As shown in figs. 4(a) and 4(b), the peak area ratio of sp² C–C bonding decreased from 63.3% to 57.9% because of the proton-irradiation-induced defects, which is in good agreement with the results for graphene subjected to helium ion bombardment.⁴⁶ The peak area ratios of C–O ($E_B = 285.3$

eV) and C=O for the proton-irradiated graphene increased from 19.4% and 1.9% to 25.6% and 3.6%, respectively. The p-type doping effects can be attributed to the charge transfer between the C bonds and the environmental molecules including oxygen and vapor.⁴⁷ Especially, the interaction between the graphene and the environmental molecules can be enhanced by the defect-induced modification of the C bonds in graphene.⁴⁸ Therefore, we believe that passivation of the graphene using inert materials can minimize the charge transfer when it is exposed to high-energy proton irradiation.

4. Conclusion

The dependence of radiation-induced damage in monolayer graphene on both the proton energy and dose was systematically investigated by applying various energies and doses and using micro-Raman spectroscopy and XPS. The increase in I_D/I_G and wider FWHM of the G peak indicated that the disorder in the graphene increased with increasing the proton dose and energy. Defect formation energies of various defect models were compared by DFT calculation. Also, we observed that electron-withdrawing molecules were adsorbed on proton-irradiated graphene, making the damaged graphene p-type after proton irradiation.

Acknowledgments

This research was supported by grants from the Basic Science Research Program (2012R1A1A2042761), the Radiation Technology Research and Development program (2013M2A2A6043608) through the National Research Foundation of Korea funded by the

Ministry of Science, Information Communication Technology & Future Planning and the
2013 Research Fund of the University of Seoul for Jeong Woo Han.

References

- [1] C. Clayes and E. Simoen, *Radiation effects in advanced semiconductor materials and devices*, Springer, 2002.
- [2] S. J. Pearton, R. Deist, F. Ren, L. Liu, A. Y. Polyakov and J. Kim, *J. Vac. Sci. Technol. A*, 2013, **31**, 050801.
- [3] A. Y. Polyakov, S. J. Pearton, P. Frenzer, F. Ren, L. Liu and J. Kim, *J. Mater. Chem. C*, 2013, **1**, 877-887.
- [4] F. Schwierz, *Nat. Nanotechnol.*, 2010, **5**, 487-496.
- [5] F. Bonaccorso, Z. Sun, T. Hasan and A. C. Ferrari, *Nat. Photonics.*, 2010, **4**, 611-622.
- [6] A. H. Reshak, S. A. Khan and S. Auluck, *J. Mater. Chem. C*, 2014, **2**, 2346-2352.
- [7] K. S. Novoselov, V. I. Fal'ko, L. Colombo, P. R. Gellert, M. G. Schwab and K. Kim, *Nature*, 2012, **490**, 192-200.
- [8] A. H. Reshak and S. Auluck, *Mater. Exp.*, 2014, **4**, 508-520.
- [9] A. H. Reshak and S. Auluck, *J. Appl. Phys.*, 2014, **116**, 103702.
- [10] A. H. Reshak, S. A. Khan and S. Auluck, *RSC Adv.*, 2014, **4**, 11967-11974.
- [11] A. Eckmann, A. Felten, A. Mishchenko, L. Britnell, R. Krupke, K. S. Novoselov and C. Casiraghi, *Nano. Lett.*, 2012, **12**, 3925-3930.
- [12] F. Banhart, J. Kotakoski and A. V. Krasheninnikov, *ACS Nano*, 2011, **5**, 26-41.
- [13] S. Wang, B. Yang, S. Zhang, J. Yuan, Y. Si, and H. Chen, *ChemPhysChem*, 2014, **15**, 2749-2755
- [14] B. Yang, S. Wang, Y. Guo, J. Yuan, Y. Si, S. Zhang and H. Chen, *RSC Adv.*, 2014, **4**, 54677- 54683.
- [15] V. A. Basiuk, K. Kobayashi, T. Kaneko, Y. Negishi, E. V. Basiuk and J.-M. Saniger-Blesa, *Nano. Lett.*, 2002, **2**, 789-791.
- [16] B. Khare, M. Meyyappan, M. H. Moore, P. Wilhite, H. Imanaka and B. Chen, *Nano. Lett.*, 2003, **3**, 643-646.
- [17] W.-K. Hong, C. Lee, D. Nepal, K. E. Geckeler, K. Shin and T. Lee, *Nanotechnol.*, 2006, **17**, 5675-5680.
- [18] S. Mathew, T. K. Chan, D. Zhan, K. Gopinadhan, A. R. Barman, M. B. H. Breese, S. Dhar, Z. X. Shen, T. Venkatesan and J. T. L. Thong, *J. Appl. Phys.*, 2011, **110**, 084309.

- [19] S. Mathew, T. K. Chan, D. Zhan, K. Gopinadhan, A.-R. Barman, M. B. H. Breese, S. Dhar, Z. X. Shen, T. Venkatesan and J. T. L. Thong, *Carbon*, 2011, **49**, 1720-1726.
- [29] G. Ko, H.-Y. Kim, F. Ren, S. J. Pearton and J. Kim, *Electrochem. Solid State Lett.*, 2010, **13**, K32-K34.
- [21] G. Kresse and J. Furthmüller, *Phys. Rev. B*, 1996, **54**, 11169-11186.
- [22] D. S. Sholl and J. A. Steckel, *Density functional theory: a practical introduction*, John Wiley & Sons, 2009.
- [23] J. P. Perdew, K. Burke and M. Ernzerhof, *Phys. Rev. Lett.*, 1996, **77**, 3865-3868.
- [24] H. J. Monkhorst and J. D. Pack, *Phys. Rev. B*, 1976, **13**, 5188-5192.
- [25] S. Grimme, *J. Comput. Chem.*, 2006, **27**, 1787-1799.
- [26] C. G. Van de Walle and J. Neugebauer, *J. Appl. Phys.*, 2004, **95**, 3851-3879.
- [27] Y. Hao, Y. Wang, L. Wang, Z. Ni, Z. Wang, R. Wang, C. K. Koo, Z. Shen and J. T. L. Thong, *Small*, 2010, **6**, 195-200.
- [28] A. C. Ferrari and D. M. Basko, *Nat. Nanotechnol.*, 2013, **8**, 235-246.
- [29] A. C. Ferrari, S. E. Rodil and J. Robertson, *Phys. Rev. B*, 2003, **67**, 155306.
- [39] H. Liu, Y. Liu and D. Zhu, *J. Mater. Chem.*, 2011, **21**, 3335-3345.
- [31] A. Das, S. Pisana, B. Chakraborty, S. Piscanec, S. K. Saha, U. V. Waghmare, K. S. Novoselov, H. R. Krishnamurthy, A. K. Geim, A. C. Ferrari and A. K. Sood, *Nat. Nanotechnol.*, 2008, **3**, 210-215.
- [32] B.-J. Kim, G. Yang, H.-Y. Kim, K. H. Baik, M. A. Mastro, J. K. Hite, C. R. Eddy, Jr., F. Ren, S. J. Pearton and J. Kim, *Opt. Express*, 2013, **21**, 29025-29030.
- [33] A. C. Ferrari and J. Robertson, *Phys. Rev. B*, 2001, **64**, 075414.
- [34] L. G. Cançado, A. Jorio, E. H. M. Ferreira, F. Stavale, C. A. Achete, R. B. Capaz, M. V. O. Moutinho, A. Lombardo, T. S. Kulmala and A. C. Ferrari, *Nano Lett.*, 2011, **11**, 3190-3196.
- [35] J. C. Meyer, C. Kisielowski, R. Erni, M. D. Rossell, M. F. Crommie and A. Zettl, *Nano Lett.*, 2008, **8**, 3582-3586.
- [36] L. Li, S. Reich and J. Robertson, *Phys. Rev. B*, 2005, **72**, 184109.
- [37] O. V. Yazyev, I. Tavernelli, U. Rothlisberger and L. Helm, *Phys. Rev. B*, 2007, **75**,

115418.

[38] J. Ma, D. Alfè, A. Michaelides and E. Wang, *Phys. Rev. B*, 2009, **80**, 033407.

[39] M. M. Ugeda, I. Brihuega, F. Guinea and J. M. Gómez-Rodríguez, *Phys. Rev. Lett.*, 2010, **104**, 096804.

[40] J. Kotakoski, A. V. Krasheninnikov, U. Kaiser and J. C. Meyer, *Phys. Rev. Lett.*, 2011, **106**, 105505.

[41] A. Hashimoto, K. Suenaga, A. Gloter, K. Urita and S. Iijima, *Nature*, 2004, **430**, 870-873.

[42] Y. Asayama, M. Yasuda, K. Tada, H. Kawata and Y. Hirai, *J. Vac. Sci. Technol. B*, 2012, **30**, 06FJ02.

[43] M. Yamamoto, Y. Asayama, M. Yasuda, H. Kawata and Y. Hirai, *J. Vac. Sci. Technol. B*, 2014, **32**, 06FK01.

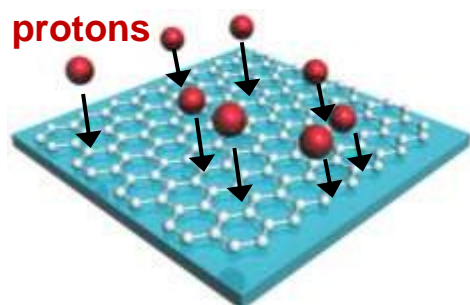
[44] D. Yang, A. Velamakanni, G. Bozoklu, S. Park, M. Stoller, R. D. Piner, S. Stankovich, I. Jung, D. A. Field, C. A. Ventrice Jr. and R. S. Ruoff, *Carbon*, 2009, **47**, 145-152.

[45] T. Zhou, F. Chen, K. Liu, H. Deng, Q. Zhang, J. Feng and Q. Fu, *Nanotechnol.*, 2011, **22**, 045704.

[46] J. -H. Kim, J. H. Hwang, J. Suh, S. Tongay, S. Kwon, C. C. Hwang, J. Wu and J. Y. Park, *Appl. Phys. Lett.*, 2013, **103**, 171604.

[47] H. Chen and E. Ruckenstein, *J. Phys. Chem. Lett.*, 2014, **5**, 2979-2982

[48] Y.-H. Zhang, Y.-B. Chen, K.-G. Zhou, C.-H. Liu, J. Zeng, H.-L. Zhang and Y. Peng, *Nanotechnol.*, 2009, **20**, 185504.



The dependence of radiation-induced damage in monolayer graphene on both the proton energy and dose was systematically investigated.